Number 3 Volume 16 September 2010 Journal of Engineering

DAMAGE DETECTION IN ROTATING BLADE BY VIBRATIONAL ANALYSIS USING FINITE ELEMENT METHOD

Dr.Nabil H. H.
Univ. of Baghdad
College of Eng.

Shwan A. Z.
Univ. of Baghdad
College of Eng.

ABSTRACT

The development of monitoring systems for rotating blade has been driven by a desire to reduce the maintenance costs and human interaction to improve the safety, reliability and operational life, so it is urgent to monitor the integrity of a structural systems. In this study four different coordinate system has been used to describe the blade motion, then an element stiffness and mass matrices has been formulated by using Hamilton's principle and finite element method, where each element has been described by seven degrees of freedom, so the method has been demonstrated analytically on a finite element model to estimate the modal parameters under rotating and non-rotating conditions in vacuum (to eliminate aerodynamic effect and damping coefficient) and to capture centrifugal effect, so the damage has been simulated by stiffness reduction of assumed elements and by crack form . These results was reasonable, so many parameters has been investigated such as, damage severity, damage location and the effect of rotation speed on these methods have been studied, as well as an assessment has been provided for these methods via statistic to suggest the effective method and this is the main objective, so The Residual Error Method was the best,compared with other methods. All formulations and computations has been coded in MATLAB version 7.

الخلاصة:

حصل التطوير في مراقبة الريش الدوارة لتقليل كلفة الصيانة وتقليل استخدام الايدي العاملة لتحسين ظروف السلامة والمحافظة على العمر الافتراضي للريشة , لذا كان من الضروري مراقبة كمالية الريشة.

استخدمت في هذه الدراسة اربعة Coordinate Systems لوصف حركية الريشة ومن ثم صياغة مصفوفتي الجساءة والكتلة باستخدام مبدأ Hamilton Principle وطريقة العناصر المحددة FEMمحاور , حيث ان كل عنصر يحوي سبع درجات من هاملتون

الحرية, وبهذا استخدم الحل العددي لحساب الترددات الطبيعية واشكالها الاهتزازية اثناء سكون الريشة واثناء دورانها في الفراغ (لتقليل تأثيرقوة الهواء) و ألتماس تأثير القوة الطاردة المركزية, ومن ثم تمثيل الضرر في الريشة على شكل نقصان في الجساءة وعلى شكل شقوق Cracks .

بالاعتماد على الترددات الطبيعية واشكالها الأهتزازية تم استخدام عدة طرق لكشف الأضرار وذلك باستخدام سيناريوهات خاصة بهذه الاضرار ومواقعها على الريشة.

تـم التوصل الى نـتـــائـــج مـعـقولة , وقد تم دراســـة بـعـض المتغيرات مثل شدة الضرر , موقعه وتأثير سرعـــة دوران الريشـة على طرق الكشف المستخدمة , ومن ثم تقييم هـذه الطـرق لاقتراح الطـريقـــة الفعالة وهذا هو الـــغرض الرئيسي من هـذه الـدراسـة, تـم اسـتـخـدام بـرنامج الحاسبةMATLAB7 كمـا تـم الوصـول الى استنتـــاجـات مقبولة ايضـا.

KEYWORDS: Damage, Rotating blade, Finite element method.

INTRODUCTION:

In the past few years the problem of health monitoring and fault detection of structures has received considerable consideration. It was noted that fault causes changes in the dynamic response of the structure, so the change can be considered as an indication of damage in a structure, consequently the scheme of fault detection are based on the comparison of the dynamic response of healthy structure with the dynamic response of defected structure.Vibration analysis has been found as an important tool in the investigations of the dynamical behavior of many industrial applications like many types of rotating blade such as axial fan, impeller, turbine, helicopter and wind turbine blades … etc.

Blade failure normally occurs when the blade is vibrating at or near resonant condition and there are many factors that can induce a damage in a mechanical structure such as , a general environmental attacks, erosion, corrosion, creep, fatigue, where the fact that many factors can contribute to form a crack (**Al-said** et al 2006), so it is the most common type of defects that occurs in structures(**Mohammad** and **Omar** 2003).

A crack in a structure introduces a local flexibility which is a function of the crack depth, and this flexibility changes the stiffness and the dynamic behavior of the structure (**Ricci** and **Viola** 2002) , so numerous attempts to quantify local defects are reported to the literature, generally the damage reduce the natural frequencies of a structure because it becomes more flexible, where this fact had been extensively used to detect the presence of damage in a structural component, so the damage is simulated by reducing the stiffness of assumed elements and by crack form also.

An important factor which based on damage detection research is the implementation of reasonable damage models. The models must accurately reflect the physics of the damage, and be compatible with the damage evaluation techniques which discussed in chapter five. Although there are many ways in which the rotor system can be damaged, this work will be limited to two categories of faults:

1- Distributed stiffness faults. 2-Cracks.

The global stiffness matrix has been developed for the eigenvalue problem (**Herrera** 2005).

BLADE KINEMATICS AND COORDINATE SYSTEMS:

Four different coordinate system are used to describe the blade motion. These coordinate systems, as listed, are the inertial, hub-fixed, undeformed-blade and deformed-blade coordinate systems. The inertial coordinate system (X_1, Y_1, Z_1) with unit vectors $\hat{I}_1, \hat{J}_1, \hat{k}_1$ is a ground-fixed reference frame and there is no fuselage motion and the hub fixed coordinate system (X_H, Y_H, Z_H) with unit vectors $\hat{I}_H$, $\hat{J}_H$, $\hat{k}_H$ is assumed parallel to the inertial coordinate system, as shown in Fig. (1) .

Z_1 Z_H

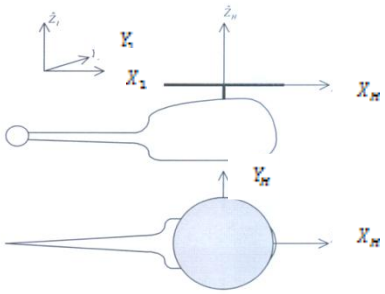

Fig. (1) Inertial and hub fixed coordinate system

The undeformed-blade coordinate system(x,y,z)with unit vectors $\hat{\imath}, \hat{\jmath}, \hat{k}$ is attached to the undeformed blade. The *z* axis of the undeformed-blade coordnate is parallel to the Z_H axis of the hub fixed coordinate system and the blade is rotating about this axis at a constant angular velocity Ω, as in Fig.(2) as well as the x-axis lies along the blade elastic axis and the *y*-axis is in the plane of rotation. In some rotor systems the equilibrium flap position is not parallel to the hub plane and this "precone" is incorporated to relieve stress in the blade root, so precone angle is neglected in this derivation because it is very small (**Hodges** and **Dowell** 1974). The transformation between the hub-fixed non-rotating and undeformed-blade coordinate systems is defined as:

$$\begin{Bmatrix} \hat{\imath} \\ \hat{\jmath} \\ \hat{k} \end{Bmatrix} = \begin{bmatrix} \cos\psi & \sin\psi & 0 \\ -\sin\psi & \cos\psi & 0 \\ 0 & 0 & 1 \end{bmatrix} \begin{Bmatrix} \hat{I}_H \\ \hat{J}_H \\ \hat{k}_H \end{Bmatrix} = T_{UH} \begin{Bmatrix} \hat{I}_H \\ \hat{J}_H \\ \hat{k}_H \end{Bmatrix} \quad (1)$$

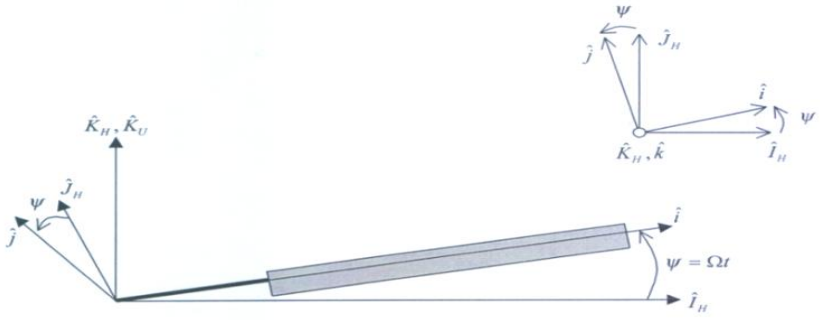

Fig. (2) Transformation between hub and undeformed blade coordinate systems

The final coordinate system to discuss is the deformed-blade coordinate system (ξ, η, ζ) with unit vectors $\hat{\imath}_\xi, \hat{\jmath}_\eta, \hat{k}_\zeta$. The transformations to get this last coordinate system is shown in Fig.(3).The elastic axis undergoes flap deflection, which contributes both a translation (*w*) and then undergoes a negative rotation(*w'*), about the undeformed-blade axis-*y* , as shown in Fig. (3 a) . At this point the blade elastic axis is coincident with the ξ axis of the deformed-blade coordinate system, then the blade cross section undergoes twist (θ_1) about the elastic axis ξ, as shown in Fig.(3 b), where the total blade pitch θ_1 is expressed as:

$$\theta_1 = \theta_0 + \phi \quad (2)$$

Where Θ_0 is the pitch angle due to control and it is very small, and Φ is the elastic twist.

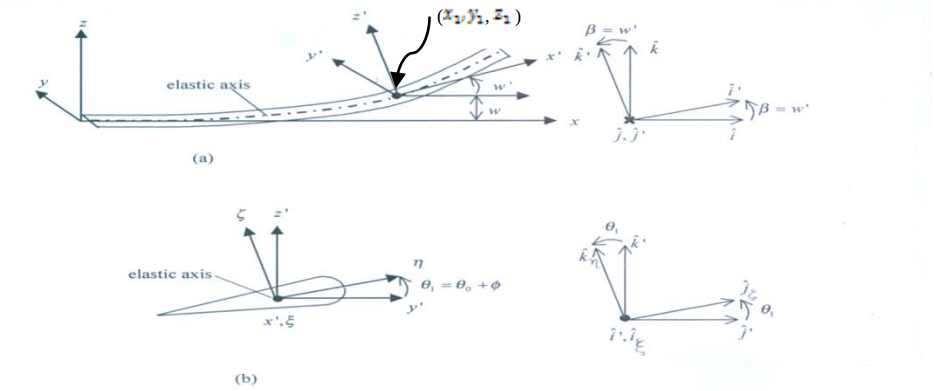

Fig. (3) Transformations from undeformed-blade to deformed-blade coordinate systems and blade cross section coordinate system

The transformation from the deformed-blade to undeformed-blade coordinate systems as in Fig. (3) is given as following(**Stevens** 2001):

$$\begin{Bmatrix} \hat{\imath} \\ \hat{\jmath} \\ \hat{k} \end{Bmatrix} = \begin{bmatrix} \cos\beta & -\sin\beta\sin\Theta & -\sin\beta\cos\Theta \\ 0 & \cos\Theta & -\sin\Theta \\ \sin\beta & \cos\beta\sin\Theta & \cos\beta\cos\Theta \end{bmatrix} \begin{Bmatrix} \hat{\imath}_\xi \\ \hat{\jmath}_\eta \\ \hat{k}_\zeta \end{Bmatrix} = T_{UD} \begin{Bmatrix} \hat{\imath}_\xi \\ \hat{\jmath}_\eta \\ \hat{k}_\zeta \end{Bmatrix} \tag{3}$$

Where β and Θ are Euler angle and can be approximated by Eq. (4).

$$\cos\beta = \sqrt{1 - w'^2} \quad , \quad \sin\beta = w' \quad , \quad \Theta = \Theta_1 \tag{4}$$

Substituting these approximations into Eq.(3) yields a more useful form of the transformation from deformed to undeformed coordinate systems, and by using local linear approximation .

$$T_{UD} = \begin{bmatrix} \left(1 - \frac{w'^2}{2}\right) & -w'\sin\Theta_1 & -w'\cos\Theta_1 \\ 0 & \cos\Theta_1 & -\sin\Theta_1 \\ w' & \left(1 - \frac{w'^2}{2}\right)\sin\Theta_1 & \left(1 - \frac{w'^2}{2}\right)\cos\Theta_1 \end{bmatrix} \tag{5}$$

The origin of the deformed - blade coordinate system is the blade elastic axis, and a chordwise locations must be defined relative to this point, as shown in Fig.(4), where the center of gravity is at a distance (*eg*) from the elastic axis; and (*eg*) is assumed positive forward.

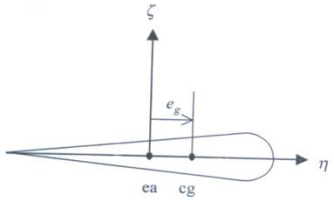

Fig. (4) The location of elastic axis and center of gravity on the chord

HAMILTON'S PRINCIPLE:

Hamilton's principle is used to derive the finite element equations to describe the rotor systems. Hamilton's principle for conservative systems states that the true motion of a system between two arbitrary moments in time integral of the difference between potential and kinetic energies . If the system is subject to non-conservative forces, such as the aerodynamic forces imposed , so the virtual work terms must be included , and Hamilton's Principle may be expressed as (**Hodeges** and **Dowell** 1974):

$$\delta\Pi = \int_{t_1}^{t_2}(\delta T - \delta U + \delta W)dt = 0 \quad (6)$$

Where the variation of blade strain energy δUin terms of engineering stress-strain relation, is given by:

$$\delta U = \int_0^R \iint_A (\sigma_{xx}\delta\varepsilon_{xx} + \sigma_{x\eta}\delta\varepsilon_{x\eta} + \sigma_{x\zeta}\delta\varepsilon_{x\zeta})\, d\eta d\zeta dx \quad (7)$$

$$(\sigma_{xx} = E\varepsilon_{xx} \quad , \quad \sigma_{x\eta} = G\varepsilon_{x\eta} \quad , \quad \sigma_{x\zeta} = G\varepsilon_{x\zeta}) \quad (8)$$

The engineering strains can be expressed in terms of translation displacement (w) , rotation (w'), curvature (w''), twist (ϕ), twist rate(ϕ'), also we should refer that the non-dimensional scheme is used for the ensuing derivations, where this scheme is necessary in order to increase the generality of the analysis in the numerical implementation , therefore for the flap-torsion case the non-dimensional variation in strain energy becomes (**Stevens** 2001):

$$\frac{\delta U}{m\Omega^2 R^3} = \int_0^1 (EI_{yy}(\cos\Theta_0)^2 w''\delta w'' + \frac{m\Omega^2}{2}(R^2 - x^2)w'\delta w' + GJ\phi'\delta\phi')\, ds \quad (9)$$

Where the tension is given as (**Solaiman** 1999). As well as the kinetic energy of the blade depends on the blade velocity. Since fuselage motion is not accounted for this derivation , the blade velocity is due only to the blade motion relative to the hub , as well as the derivation describes only flap and twist motion of the blade , so the position of an arbitrary point after the beam has deformed is given by (x_1, y_1, z_1), see Fig. (3)

$$\left.\begin{aligned} x_1 &= x + u - w'(\eta\sin\Theta_1 + \zeta\cos\Theta_1) \\ y_1 &= \eta\cos\Theta_1 - \zeta\sin\Theta_1 \\ z_1 &= w + \eta\sin\Theta_1 + \zeta\cos\Theta_1 \end{aligned}\right\} \quad (10)$$

Then differentiating the position vector with respect to the hub-fixed non-rotating coordinate system yield (**Stevens** 2001):

$$\overrightarrow{V_b} = \overrightarrow{V_{bx}}\hat{\imath} + \overrightarrow{V_{by}}\hat{\jmath} + \overrightarrow{V_{bz}}\hat{k} \quad (11)$$

$$\delta T = \int_0^R \iint_A \rho\overrightarrow{V_b}.\overrightarrow{\delta V_b}\, d\eta d\zeta dx \quad \text{(variation in kinetic energy)} \quad (12)$$

From Eq.(12)-(14) and via integrating by parts as in reference, the non−dimensional variation of kinetic energy becomes:

$$\frac{\delta T}{m\Omega^2 R^3} = \int_0^1 (T_w\delta w + T_{w'}\delta w' + T_\phi\delta\phi)\, ds \quad (13)$$

$$
\begin{aligned}
&T_w = -m\ddot{w} - \ddot{\phi} m e_g \cos\Theta_0 \\
&T_{w'} = -x m e_g \Omega^2 \sin\Theta_0 - \phi x m e_g \Omega^2 \cos\Theta_0 \\
&T_\phi = -\ddot{w} m e_g \cos\Theta_0 - \ddot{\phi} m k_m^2 - w' x m e_g \Omega^2 \cos\Theta_0 \\
&-m\Omega^2 (k_{m2}^2 - k_{m1}^2)\cos\Theta_0 \sin\Theta_0 - \phi m \Omega^2 (k_{m2}^2 - k_{m1}^2)\cos 2\Theta_0 \\
&m k_{m1}^2 = \iint_A \rho\, \zeta^2 \, d\eta d\zeta \; ; \; m k_{m2}^2 = \iint_A \rho\, \eta^2 \, d\eta d\zeta \; ; \; k_m = \sqrt{k_{m1}^2 + k_{m2}^2}
\end{aligned}
\qquad (14)
$$

So the virtual work δW of non-concentrative forces may be expressed as:

$$\delta W = \int_0^R (L_w^A \delta w + M_\phi^A \delta\phi) dx \qquad (15)$$

The terms due to the blade airfoil are (L_w^A), where the distributed air load in the(z)direction, and (M_ϕ^A) the aerodynamic pitching moment about undeformed elastic axis, but In this study the aerodynamic effects are not included .

BLADE FINITE ELEMENT:

The spatial finite element equations of motion are derived in this section , and the generalized Hamilton's principle must be written in the non-dimensional form, so the discredited form in Eq.(16):

$$\delta\Pi = \int_{\bar{\psi}_1}^{\bar{\psi}_2} \sum_{i=1}^{N} (\delta T_i - \delta U_i + \delta W_i) d\bar{\psi} \quad = 0 \qquad (16)$$

The blade finite element discretization is shown in Fig. (5), where the blade is discredited into N beam elements, each consisting of seven degrees of freedom , so these degrees of freedom are distributed among three nodes, two external and one internal, as well as the displacement of the left hand node is described by lateral displacement, slope and twist denoted as (w_A , w_A' and ϕ_A), likewise the displacement of the right hand node is described by (w_B , w_B' and ϕ_B), and the displacement of the internal node is described only by a twist (ϕ_M). Elemental boundary conditions requires continuity of displacement and slope of flap deflection and continuity of displacement of elastic twist.

Within each element, deformations between the nodes are described using shape functions, where these shape functions, are derived from a cubic Hermetian polynomial for flap deformation and a quadratic polynomial for torsion deformation (Rao S. S. 1989), and by using these shape functions the continuous deflections over a beam elements can be expressed in terms of the nodal displacements $\boldsymbol{q}_i$, as in Eq. (17).

$$\mathbf{u}(s) = \begin{Bmatrix} w(s) \\ \phi(s) \end{Bmatrix} = \begin{bmatrix} H_w & 0 \\ 0 & H_\phi \end{bmatrix} \boldsymbol{q}_i \qquad (17)$$

$$\mathbf{q}_i^T = [w_A \; , w_A' \; , w_B \; , \; w_B' \; , \phi_A \; , \phi_M \; , \phi_B \;] \quad \text{(elemental nodal displacement vector)} \qquad (18)$$

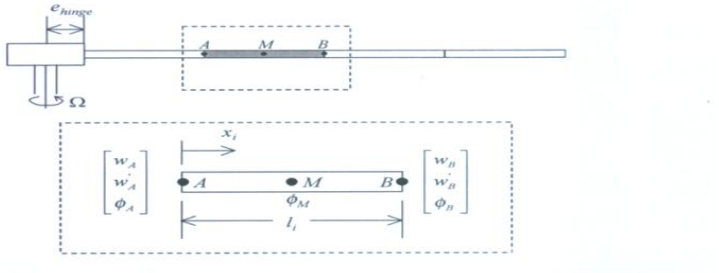

Fig. (5) Finite element discretization and elemental degrees of freedom

The polynomials for the bending and torsion shape functions are given in Eq.(19), respectively, where $s=\frac{x_i}{L_i}$ and L_i is the length of the i^{th} beam element.

$$H_w^T=\begin{Bmatrix}H_{w1}\\H_{w2}\\H_{w3}\\H_{w4}\end{Bmatrix}=\begin{Bmatrix}2s^3-3s^2+1\\l_i(s^3-2s^2+s)\\-2s^3+3s^2\\l_i(s^3-s^2)\end{Bmatrix} \quad , \quad H_\phi^T=\begin{Bmatrix}H_{\phi1}\\H_{\phi2}\\H_{\phi3}\end{Bmatrix}=\begin{Bmatrix}2s^2-3s+1\\-4s^2+4s\\2s^2-s\end{Bmatrix} \tag{19}$$

The variations in displacements (δw) and ($\delta\Phi$) can be written in terms of variations in nodal displacements as in Eq. (20).

$$\delta\mathbf{u}(s)=\begin{Bmatrix}\delta w(s)\\\delta\phi(s)\end{Bmatrix}=\begin{bmatrix}H_w & 0\\0 & H_\phi\end{bmatrix}\delta\boldsymbol{q}_i \tag{20}$$

Looking more closely at the expression for variations in strain and kinetic energies, as in Eq. (9) and (13). It is clear that the total energy also depends on ($\delta w'$,$\delta w''$ and $\delta\phi'$), so these variations are found by spatially differentiating for Eq.(20). Since the variations in nodal degrees of freedom $(\delta\boldsymbol{q}_i)$are discrete; the shape functions capture the spatial variation as in Eq. (21) , where :

$$\{\delta w'(s)\}=[H_w']\begin{Bmatrix}\delta w_A\\\delta w_A'\\\delta w_B\\\delta w_B'\end{Bmatrix} \ , \ \{\delta w''(s)\}=[H_w'']\begin{Bmatrix}\delta w_A\\\delta w_A'\\\delta w_B\\\delta w_B'\end{Bmatrix} \ , \ \{\delta\phi'(s)\}=[H_\phi']\begin{Bmatrix}\delta\phi_A\\\delta\phi_M\\\delta\phi_B\end{Bmatrix} \tag{21}$$

ELEMENTAL MATRICES:

The expressions is integrated by parts, so the mass and stiffness matrices are identified by separating acceleration, and displacement terms, then the virtual energy expression in terms of the elemental matrices becomes:

$$\delta\Pi=\int_{\bar{\psi}_1}^{\bar{\psi}_2}[\textstyle\sum_{i=1}^{N}\delta\boldsymbol{q}_i^T(\boldsymbol{M}_i^b\,\ddot{\boldsymbol{q}}_i+\boldsymbol{K}_i^b\,\boldsymbol{q}_i)]\,d\bar{\psi} \quad =0 \tag{22}$$

There are no structural contributions for damping in the preceding formulation to facilitate the simulation in *vacuum* cases, so there are no aerodynamic effects.The elemental mass and stiffness matrices can be partitioned to indicate contributions from flap bending and elastic torsion.

$$[\boldsymbol{M}_i^b]=\begin{bmatrix}M_{ww}^b & M_{w\phi}^b\\ M_{\phi w}^b & M_{\phi\phi}^b\end{bmatrix}\ ,\ [\boldsymbol{K}_i^{str}]=\begin{bmatrix}K_{ww}^{str} & K_{w\phi}^{str}\\ K_{\phi w}^{str} & K_{\phi\phi}^{str}\end{bmatrix}\ ,\ [\boldsymbol{K}_i^{CF}]=\begin{bmatrix}K_{ww}^{CF} & K_{w\phi}^{CF}\\ K_{\phi w}^{CF} & K_{\phi\phi}^{CF}\end{bmatrix} \quad (23)$$

$$[\boldsymbol{K}_i^b]=[\boldsymbol{K}_i^{str}]+[\boldsymbol{K}_i^{CF}]=\begin{bmatrix}K_{ww}^b & K_{w\phi}^b\\ K_{\phi w}^b & K_{\phi\phi}^b\end{bmatrix} \quad (24)$$

$$\left.\begin{aligned}&[M_{ww}^b]=\int_0^1 mH_w^TH_w\,ds\ ,\ [M_{\phi\phi}^b]=\int_0^1 mK_m^2H_\phi^TH_\phi\,ds \quad \text{(mass terms)}\\ &[M_{w\phi}^b]=\int_0^1 me_g\cos\Theta_0H_w^TH_\phi\,ds\ ,\ [M_{\phi w}^b]=\int_0^1 me_g\cos\Theta_0H_\phi^TH_w\,ds\end{aligned}\right\} \quad (25)$$

The blade stiffness terms will have components due to both structural and centrifugal terms, where the stiffness terms due to structural properties are:

$$[K_{ww}^{str}]=\int_0^1 EI_{yy}(\cos\Theta_0)^2H_w''^TH_w''ds\ ,\ [K_{\phi\phi}^{str}]=\int_0^1 GJH_\phi'^TH_\phi'ds\ ,\ [K_{w\phi}^{str}]=[K_{\phi w}^{str}]=0 \quad (26)$$

Since the rotor blade rotates, the centrifugal forces contribute a significant stiffening effect,where the stiffness terms due to centrifugal loading are given in Eq.(27) .

$$\left.\begin{aligned}&[K_{ww}^{CF}]=\int_0^1\frac{m\Omega^2}{2}(R^2-x^2)H_w'^TH_w'ds\ ,\ [K_{\phi\phi}^{CF}]=\int_0^1 m\Omega^2(K_{m2}^2-K_{m1}^2)\cos2\Theta_0H_\phi^TH_\phi\,ds\\ &[K_{w\phi}^{CF}]=\int_0^1 xme_g\Omega^2\cos\Theta_0H_w'^TH_\phi ds\ ,\ [K_{\phi w}^{CF}]=\int_0^1 xme_g\Omega^2\cos\Theta_0H_\phi^TH_w'ds\end{aligned}\right\} \quad (27)$$

In Eq.(27), the term $\frac{m\Omega^2}{2}(R^2-x^2)$ is the axial loading due to centrifugal forces at the location x , so in Eq.(27) x is the distance from the shaft axis to the point on the blade, where a centrifugal force will be at maximum value when $x = 0$, and a centrifugal force will be zero at $x = R$.

ASSEMBLY OF GLOBAL MATRICES:

The elemental degrees of freedom has been ordered according to flap or torsional motion, thus the order was:(w_A , w_A' , w_B , w_B' , ϕ_A , ϕ_M and ϕ_B).

Via multiplying the elemental mass and stiffness matrices by transformation matrix t_r as in Eq. (28) to get a new reordered stiffness and mass matrices for assembly .

$$[t_r]=\begin{bmatrix}1&0&0&0&0&0&0\\0&1&0&0&0&0&0\\0&0&0&0&1&0&0\\0&0&0&0&0&1&0\\0&0&1&0&0&0&0\\0&0&0&1&0&0&0\\0&0&0&0&0&0&1\end{bmatrix}\ ,\ [\mathrm{K}_{ei}]=[t_r]*[K_i^b]*[t_r]\ ,\ [\mathrm{M}_{ei}]=[t_r]*[M_i^b]*[t_r] \quad (28)$$

Where $[\mathrm{K}_{ei}]$ is reordered stiffness matrix for i^{th} element and $[\mathrm{M}_{ei}]$ is reordered mass matrix for i^{th} element, so the global matrices is more straightforward if the degrees of freedom are reordered spatially, and the reorder result becomes:(w_A , w_A' , ϕ_A , ϕ_M , w_B , w_B' , ϕ_B), so the virtual energy becomes:

$$\delta\Pi=\int_{\bar\psi_1}^{\bar\psi_2}\delta\boldsymbol{q}^T(\boldsymbol{M\ddot q}+\boldsymbol{Kq})d\bar\psi\ =0 \quad (29)$$

Since the virtual displacements $\delta \boldsymbol{q}$ are arbitrary (between any two moments), so the integrand in Eq. (29) must be vanished, then the equation of motion becomes:

$$\boldsymbol{M\ddot{q} + Kq = 0} \tag{30}$$

So the modal parameters of a blade is considered(with centrifugal effect and without centrifugal effect) for the undamaged and damaged cases. For the undamped system of several degrees of freedom , the equations of motion expressed in matrix form become:

$$[\mathbf{M}_g]\{\ddot{u}\} + [\mathbf{K}_g]\ \{u\} = \{0\} \tag{31}$$

By using the characteristic equation of the system, so the roots λ_i of the characteristic equation are called eigenvalues (Thomson W. T. 1975), so it is possible to find the eigenvectors from the adjoint matrix , and the complete free vibration solution is expressed also. The mode shape vectors has very important properties and known as the orthogonality properties which are described by (Meirovitch L. 1975), so the most common normalization scheme has been used in modal analysis to normalize the modes with respect to the mass matrix $[\mathbf{M}_g]$.The global displacement vector and matrices has been defined as:

$$\boldsymbol{q}_g = \sum_{i=1}^{N} \boldsymbol{q}_i \ , \quad \mathbf{M}_g = \sum_{i=1}^{N} \mathrm{M}_{ei} \ , \quad \mathbf{K}_g = \sum_{i=1}^{N} \mathrm{K}_{ei} \tag{32}$$

The summations represent the assembly procedure as shown in Fig.(6), where the matrix rows and columns has been reordered to facilitate assembly , then the structural mass and stiffness matrices has been banded. The assembly procedure can be easily modified to accommodate different types of rotor systems, and the assembly method which described in Fig.(5) assumes cantilevered boundary conditions between each element, so the boundary conditions between two elements states that the displacement, slope and twist are continuous at the nodes as :

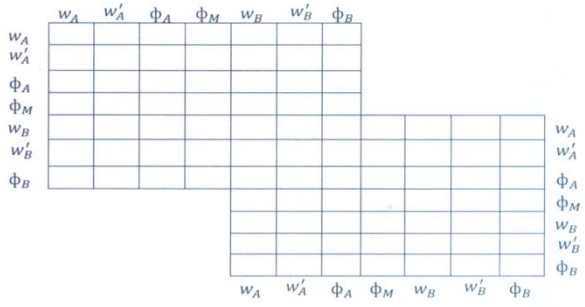

$$\left.\begin{aligned} w_A(i) &= w_B(i-1) \\ w'_A(i) &= w'_B(i-1) \\ \phi_A(i) &= \phi_B(i-1) \end{aligned}\right\} \tag{33}$$

Fig. (6) The assembly procedure

APPLICATION OF KINEMATICS BOUNDARY CONDITIONS:

Kinematic boundary conditions are applied to the global matrices, and the rotor model assumes that the blade is cantilevered at the root, so the degrees of freedom (w, w' and Φ) are constrained, and the corresponding rows and columns are removed from the FEM.

DAMAGE MODELS:

The distributed stiffness fault is modeled as a 10% and 20% reduction in blade bending and torsional stiffness, but for the crack form the damaged element of the beam is modeled with two nodes and two degrees of freedom(transverse displacement and slope) at each node, where the goal is to find a beam finite element that represents the effects of a crack in a beam as shown in Fig(8).In this study the finite element model for the cracked beam with an one-edge and non-propagating was proposed by Qian et al and also used by(**Cacciola** et al 2003), so a crack affects the bending stiffness of the blade only.

STIFFNESS MATRIX OF THE CRACKED ELEMENT:

An element stiffness matrix of a beam with a crack has been formulated and then a finite element model of a cracked beam has been developed. The strain energy of an element without a crack is:

$$W^{(0)} = \frac{1}{2EI}\int_0^l (M + Pz)^2 dz = \frac{1}{2EI}\left(M^2 l + \frac{P^2 l^3}{3} + MPl^2\right) \quad (34)$$

The flexibility coefficients are expressed by a stress intensity factor in the linear elastic range using Castigliano theorem, so the additional energy in the case of rectangular beam of height h and width b due to the crack can be written as:

$$W^{(1)} = b\int_0^a \left(\frac{K_I^2 + K_{II}^2}{E_p} + \frac{(1+\upsilon)K_{III}^2}{E}\right) da \quad (35)$$

Where $E_p = E$ for plane stress, $E_p = E/(1-\upsilon^2)$ for plane strain and(a) is the crack depth, as well as by taking into account only bending, so Eq. (35) leads to:

$$W^{(1)} = b\int_0^a \frac{(K_{IM}+K_{IP})^2 + K_{IIP}^2}{E_p} da \quad (36)$$

$$K_{IM} = \frac{6M}{bh^2}\sqrt{\pi a}\,\mathrm{F}_I(S)\ ,\ K_{IP} = \frac{3Pl}{bh^2}\sqrt{\pi a}\,\mathrm{F}_I(S)\ ,\ K_{IIP} = \frac{P}{bh}\sqrt{\pi a}\,\mathrm{F}_{II}(S) \quad (37)$$

Where K_{IM}, K_{IP}, and K_{IIP} are the stress intensity factors for opening type and sliding type of cracks, due to M and P respectively, and $\mathrm{F}_I(s)$ and $\mathrm{F}_{II}(s)$ are the correction factor , see Fig.(7).

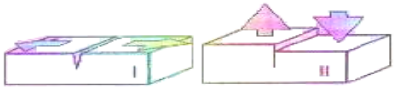

Mode I : opening mode Mode II :sliding mode
Fig. (7) The modes of loading

$$\mathrm{F}_I(s) = \sqrt{\left(\frac{2}{\pi s}\right)\tan\left(\frac{\pi S}{2}\right)}\,\frac{0.923 + 0.199[1-\sin(\frac{\pi S}{2})]^4}{\cos(\frac{\pi S}{2})}\ ,\ \mathrm{F}_{II}(s) = (3S - 2S^2)\frac{1.122 - 0.561S + 0.085S^2 + 0.18S^3}{\sqrt{1-S}} \quad (38)$$

Where (S) is the ratio between crack depth and height of element (a/h), so the elements of the flexibility matrix $c_e^{(0)}$ of the undamaged element can be derived as :

$$c_e^{(0)} = \frac{\partial^2 W^{(0)}}{\partial P_i \partial P_j} ; \quad i,j = 1,2 \qquad P_1 = P \, , \; P_2 = M \tag{39}$$

And the element of the additional flexibility matrix $c_e^{(1)}$ are :

$$c_e^{(1)} = \frac{\partial^2 W^{(1)}}{\partial P_i \partial P_j} ; \quad i,j = 1,2 \qquad P_1 = P \, , \; P_2 = M \tag{40}$$

Finally the total flexibility matrix for the element with a crack is :

$$c_e = c_e^{(0)} + c_e^{(1)} \tag{41}$$

From equilibrium conditions the following matrix has been found:

$$[\boldsymbol{T}] = \begin{bmatrix} -1 & -L & 1 & 0 \\ 0 & -1 & 0 & 1 \end{bmatrix}^T \tag{42}$$

From the principle of virtual work the stiffness matrix of cracked element can be written as :

$$[K_c] = \boldsymbol{T}\, c_e^{-1}\, \boldsymbol{T}^T \quad , \quad [K_u] = [K_{ww}^{str}] = \boldsymbol{T}\, c_e^{(0)-1}\, \boldsymbol{T}^T \tag{43}$$

Then the stiffness matrix of cracked element can be written as:

$$[K_c] = [K_{ww}^{str}] \tag{44}$$

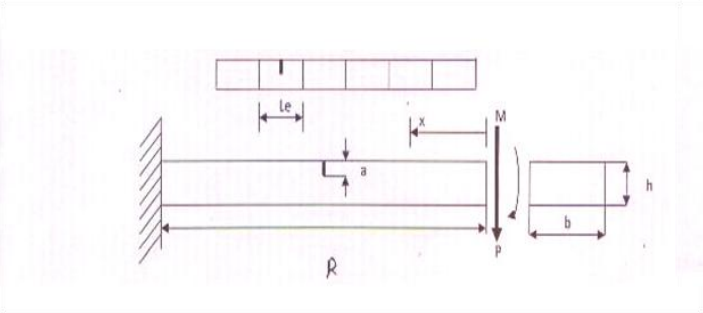

Fig. (8) Cracked cantilever

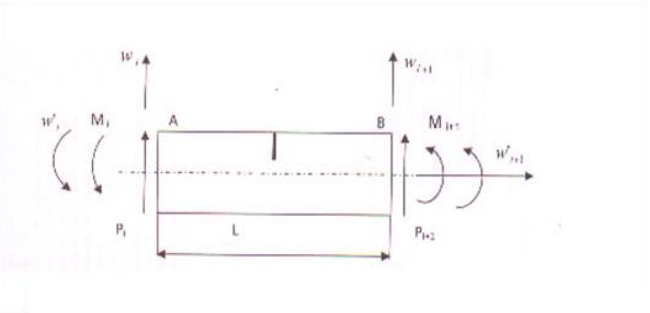

Fig. (9) Equilibrium conditions of a cracked element

Then:

$$[K_i^{str*}] = \begin{bmatrix} K_c & K_{w\phi}^{str} \\ K_{\phi w}^{str} & K_{\phi\phi}^{str} \end{bmatrix} \quad , \quad [K_i^{CF}] = \begin{bmatrix} K_{ww}^{CF} & K_{w\phi}^{CF} \\ K_{\phi w}^{CF} & K_{\phi\phi}^{CF} \end{bmatrix} \tag{45}$$

$$[K_i^{b*}] = [K_i^{str*}] + [K_i^{CF}] = \begin{bmatrix} K_{ww}^{b} & K_{w\phi}^{b} \\ K_{\phi w}^{b} & K_{\phi\phi}^{b} \end{bmatrix} \quad , \quad [K_{ei}^*] = [t_r] * [K_i^{b*}] * [t_r] \tag{46}$$

Where $[K_{ei}^*]$ is the reordered stiffness matrix for i^{th} cracked element, and as mentioned that the damage does not alter the mass of the structure, so :

$$[M_{ei}^{*}] = [M_{ei}] \quad (47)$$

DAMAGE EFFECT ON MODAL PARAMETERS :

The free vibration analysis of a blade with and without damage has been performed, so the cantilever beam is an idealized model for a blade which described. The stiffness and mass matrices will be used for a simple model of blade for analytical study . The following dimensions and material properties of the aluminum blade are listed in table (1) .

Table (1) Material properties of the blade

Blade length (R)	0.594 m
Blade width (b)	0.037 m
Blade height (h)	0.0015 m
Modulus of elasticity (E)	62.1 GPa
Modulus of rigidity (G)	23.3 GPa
Mass density (ρ)	2700 Kg/m^3
Poisson's ratio (υ)	0.34

DAMAGE SCENARIOS:

20 damage scenarios has been investigated and summarized in table (2), where in 1^{st} 10 scenarios the damage has been simulated by stiffness reduction of assumed elements, and in 2^{nd} 10 scenarios the damage has been simulated in the form of crack, so the finite element model of the blade has been used for the stiffness matrix of the cracked element which described in chapter three. For the finite element analysis the blade has been divided into 20 elements to locate the damage accurately.

Table (2) Damage scenarios

Damage scenarios	Damaged element	Stiffness reduction %	a/h
D1	1^{st} (0-0.0297)m	10	-
D2	1^{st} (0-0.0297)m	20	-
D3	5^{th} (0.1188-0.1485)m	10	-
D4	5^{th} (0.1188-0.1485)m	20	-
D5	10^{th} (0.2673-0.297)m	10	-
D6	10^{th} (0.2673-0.297)m	20	-
D7	15^{th} (0.4158-0.4455)m	10	-
D8	15^{th} (0.4158-0.4455)m	20	-
D9	5^{th} & 10^{th}	10	-
D10	5^{th} & 10^{th}	20	-
C1	1^{st} (0-0.0297)m	-	0.1
C2	1^{st} (0-0.0297)m	-	0.2
C3	5^{th} (0.1188-0.1485)m	-	0.1
C4	5^{th} (0.1188-0.1485)m	-	0.2
C5	10^{th} (0.2673-0.297)m	-	0.1
C6	10^{th} (0.2673-0.297)m	-	0.2
C7	15^{th} (0.4158-0.4455)m	-	0.1
C8	15^{th} (0.4158-0.4455)m	-	0.2
C9	5^{th} & 10^{th}	-	0.1
C10	5^{th} & 10^{th}	-	0.2

ROTATION SPEED EFFECTS ON MODAL PARAMETERS :

The purpose of this section is to study the centrifugal effect on detection methods, so four rotation speed scenarios has been assumed for two speed of rotation as listed in table (3), where the first two scenarios associated with the stiffness reduction conditions and the second two scenarios associated with the crack conditions .

Table (3) Rotation speed scenarios

Rotation speed scenarios	Damaged element	a/h	Stiffness reduction %	Ω rad/sec
SD1	5^{th} (0.1188-0.1485)m	-	20	0
SD2	5^{th} (0.1188-0.1485)m	-	20	30
SC1	5^{th} (0.1188-0.1485)m	0.2	-	0
SC2	5^{th} (0.1188-0.1485)m	0.2	-	30

METHODS OF DAMAGE DETECTION:

These techniques commonly employed are based on vibration measurement, so in these methods the damage has been detected from alternations in dynamic parameters for healthy and damaged states , so these methods are :

1. Methods based on changes in frequencies and mode shapes like:
   a. Changes in Natural Frequencies .
   b. Eigenparameter Method .
   c. Residual Error Method in The Movement Equation .
2. Methods Based on The Mode Shape Curvature (Mode Shape Curvature Method).

A. CHANGE IN NATURAL FREQUENCIES :

Modal frequency shift was presented as a common damage indicator , this section explores the applications and limitations of using modal frequency shifts as damage indicators in rotating blade, where the eigenvalue problem of the undamaged and damaged structure has been estimated by using characteristic equation (**Thomson** 1975) .

B. EIGENPARAMETER METHOD :

The eigenparameter method was proposed by(**Yuen** 1984), to detect and locate the damage in a cantilever beam, so the eigenequation for undamaged and damaged cantilever can be written as:

$$([\mathbf{K}_g] - \lambda_i[\mathbf{M}_g])\{u_N^{(i)}\} = 0 \;\; ; \;\; ([\mathbf{K}_g^*] - \lambda_i^*[\mathbf{M}_g^*])\{u_N^{(i)*}\} = 0 \qquad (48)$$

The eigenvalue is chosen in normalized form of damage, and the following eigenparameters has been estimated in the analysis :

$$\{\boldsymbol{U}_i\} = \frac{\{u_N^{(i)*}\}}{\lambda_i^*} - \frac{\{u_N^{(i)}\}}{\lambda_i} \quad (49)$$

C. RESIDUAL ERROR METHOD IN THE MOVEMENT EQUATION:

The Residual error method in the movement equation was proposed by Genovese, and also used by (**Brasiliano** 2003). This method is used to identify a damage present in a structure and locate it by observing the error present in the movement equation:

$$\boldsymbol{Er}=[\mathbf{K}_g][u^*] - ([\mathbf{M}_g][u^*])[\Lambda^*] \quad (50)$$

$$\boldsymbol{Er}= [\, e_1\, e_2\, e_3\, e_4 \ldots\ldots\ldots\ldots e_n] \quad (51)$$

$$[u^*]=[\{u^{(1)*}\}\,\{u^{(2)*}\}\,\{u^{(3)*}\}\,\ldots\ldots\ldots\{u^{(n)*}\}] \quad (52)$$

$$[\Lambda^*] = \begin{bmatrix} \omega_{n1}^{2*} & 0 & \ldots & 0 \\ 0 & \omega_{n2}^{2*} & \cdots & 0 \\ \vdots & \vdots & \ddots & \vdots \\ 0 & 0 & \cdots & \omega_{ni}^{2*} \end{bmatrix} \quad (53)$$

Each column of matrix ***Er*** is a vector corresponding to one mode shape and each value of this vector represents the error that occurs in some positions of the blade.

MODE SHAPE CURVATURE :

This method was proposed by (**Pandey** et al.1991) , and also used by (**Herrera** 2005) , so this method demonstrate that the absolute changes in mode shape curvature can be used as a good indicator for damage presence of FEM beam structures. The curvature values has been computed from the displacement mode shape by using the central difference approximation for mode *i* and DOF q:

$$\{u_N^{(i)''}\}=\frac{\{u_N^{(i)}\}_{q-1}-2\{u_N^{(i)}\}_q+\{u_N^{(i)}\}_{q+1}}{L_e^2}\;;\;\{u_N^{(i)''*}\}=\frac{\{u_N^{(i)*}\}_{q-1}-2\{u_N^{(i)*}\}_q+\{u_N^{(i)*}\}_{q+1}}{L_e^2} \quad (54)$$

$$\left\{\Delta\, u_N^{(i)''}\right\}=\left|\left\{u_N^{(i)''*}\right\}-\left\{u_N^{(i)''}\right\}\right| \quad (55)$$

RESULTS AND DISCUSSION:

The present study is based on bending mode only, where the cracked element associated with the bending mode and only the translation degrees of freedom along the perpendicular axis to the elements (vertical **DOF** in the blade)has been considered,where the rotation degrees in an experimental work are not obtained because of the difficulty in their measurement. As well as the torsion mode affected by rotation speed less than bending mode, for these reasons this study is concentrated on the bending.

DAMAGE EFFECT ON MODAL PARAMETERS :

The first five natural frequencies for the blade at $\Omega = 0$ (rad/sec) and at $\Omega = 30$ (rad/sec) has been tabulated in tables (4) and (5) for assumed scenarios.

Table (4) Natural frequencies for the blade at $\Omega = 0$ (rad/sec)

scenarios	1st mode	2nd mode	3rd mode	4th mode	5th mode
Present undamaged	20.6939	129.6868	363.1318	711.6263	1176.5
D1	20.4826	128.5971	360.5878	707.5026	1170.8
D2	20.2271	127.3253	357.7042	702.9457	1164.7
D3	20.5847	129.68	362.13	708.3462	1173.8
D4	20.4506	129.6717	360.9180	704.4352	1170.7
D5	20.6626	128.9964	363.0529	708.1019	1175.5
D6	20.6236	128.1537	362.956	703.8758	1174.3
D7	20.6908	129.3639	360.8984	709.054	1176.2
D8	20.6868	128.9621	358.1819	706.01	1175.8
D9	20.6272	129.3548	362.6206	708.3669	1174.7
D10	20.5539	128.9901	362.0612	704.8110	1172.9
C1	20.6851	129.6410	363.0250	711.4557	1176.3
C2	20.6592	129.5061	362.7112	710.9558	1175.6
C3	20.6894	129.6867	363.0910	711.4889	1176.4
C4	20.6761	129.6865	362.9703	711.0838	1176.1
C5	20.6926	129.6581	363.1296	711.4793	1176.5
C6	20.6888	129.5736	363.1229	711.0457	1176.4
C7	20.6938	129.6735	363.0391	711.5199	1176.5
C8	20.6934	129.6344	362.7652	711.2064	1176.5
C9	20.6881	129.6581	363.0887	711.3419	1176.4
C10	20.671	129.5733	362.9615	710.5092	1175.9
Frequency decreasing%	0-2.3	0-1.85	0-1.51	0-1.23	0-1.01

Table (5) Natural frequencies for the blade at $\Omega = 30$ (rad/sec)

Scenarios	1st mode	2nd mode	3rd mode	4th mode	5th mode
Undamaged	38.4810	150.5482	384.6151	734.0786	1199.6
D1	38.2927	149.5488	382.1778	730.0604	1194
D2	38.0690	148.3912	379.4244	725.6270	1188
D3	38.4343	150.5407	383.7020	730.9727	1196.9
D4	38.3774	150.5314	382.5917	727.2765	1193.9
D5	38.4732	149.9810	384.5330	730.7424	1198.5
D6	38.4635	149.2921	384.4325	726.7488	1197.3
D7	38.4804	150.2511	382.4578	731.6352	1199.3
D8	38.4795	149.8832	379.8411	728.7463	1198.9
D9	38.4550	150.2743	384.1418	730.9915	1197.8
D10	38.4266	149.9741	383.6247	727.6265	1195.9
C1	38.4732	150.5061	384.5129	733.9127	1199.3
C2	38.4499	150.3824	384.2125	733.4265	1198.7
C3	38.4791	150.5480	384.5776	733.9484	1199.4
C4	38.4734	150.5476	384.4669	733.5645	1199.1
C5	38.4807	150.5246	384.6126	733.9394	1199.5
C6	38.4798	150.4550	384.6053	733.5288	1199.4
C7	38.4810	150.5360	384.5255	733.9777	1199.6
C8	38.4809	150.4999	384.2606	733.6803	1199.5

C9	38.4788	150.5245	384.5751	733.8092	1199.4
C10	38.4721	150.4545	384.4571	733.0145	1199
Frequency decreasing%	0-1.07	0-1.43	0-1.34	0.013-1.15	0-0.97

The shifting in natural frequencies at (Ω=30 rad/sec)is smaller than the shift at (Ω=0 rad/sec)where the centrifugal effect stiffening the blade so the effect of damage becomes smaller, so the indication for damage presence is clearest at (Ω=0 rad/sec). It is clear also that the maximum shifting occurred at the scenario D2(clearest scenario as it has been mentioned) for the first five natural frequencies where D2 has the severest damage value and the nearest damaged element to the fixed end.

DAMGE SEVERITY EFFECT:

The first three natural frequencies have been observed for variant damage severity (from 5% to 60% stiffness reduction and crack depth) at 1st element. It was observed that 1st natural frequencies decrease when the damage severity(stiffness reduction,crack depth)increase, and it was observed also that the, so it is clear also from Fig.(10)that the natural frequencies affected by stiffness reduction more than crack.

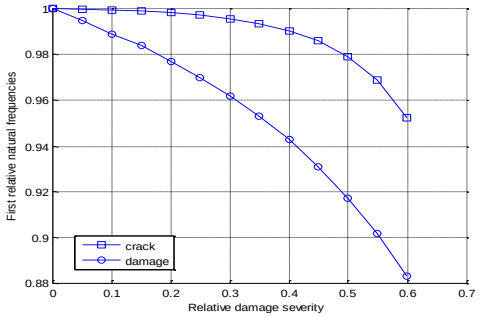

Fig.(10) Relative natural frequencies and relative damage severity and crack depth (1st mode)

ROTATION SPEED EFFECT ON NATURAL FREQUENCIES FOR UNDAMAGED BLADE:

In order to investigate the effect of the rotation speed nine values have been used (10- 90)rad/sec, and it was clear from Fig.(11) that the natural frequencies increase by rotational speed increasing where the centrifugal force stiffening the blade (due to presence of K^{CF} terms).

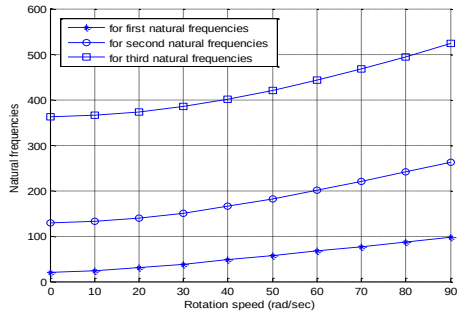

Fig. (11) The relation between natural frequencies and rotation speed

CHANGES IN NATURAL FREQUENCIES:

The measurement of natural frequencies is the first method to detect the damage, so the results have been tabulated in tables(4)and (5). It is clear from these results that the shifting in natural frequencies

is insufficient detection indicator especially at Ω=30 (rad/sec), so changes in natural frequencies being more small when the damaged zone shifted toward free end.

EIGENPARAMETER METHOD:

For the first mode the slope starts at the damaged location and this slope becomes steeper when the damaged location shifted closer to the fixed end, where the maximum bending has been occurred at this point and when the damage being more sever as shown in Fig.(12)and(13). This method is efficient for damage identification for the cases of single damages. In the cases of multiple damage the method is ineffective, where this method is able to locate the damage at one location only, as shown in Fig.(14) and (15).

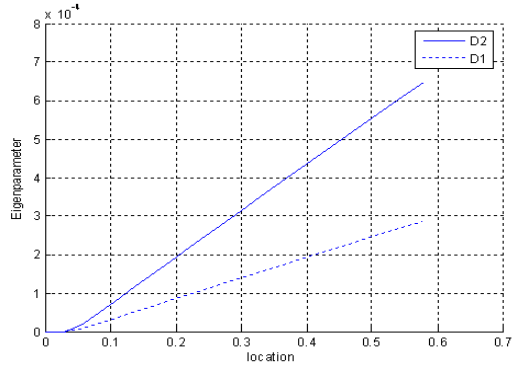

Fig(12) Eigenparameter for D1,D2 (1st mode)

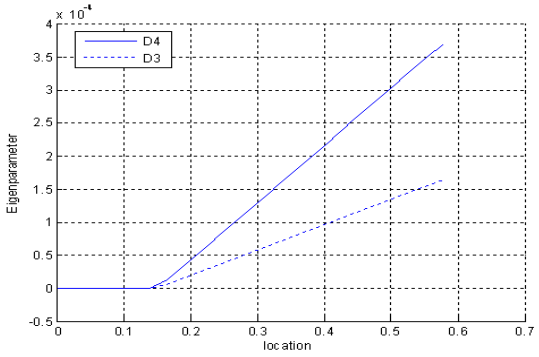

Fig.(13) Eigenparameter for D3,D4 (1st mode)

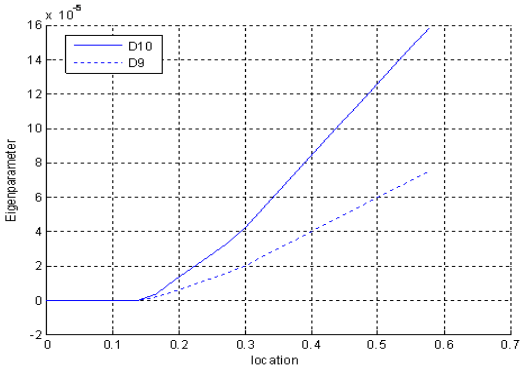

Fig.(14) Eigenparameter for D9,D10 (1st mode)

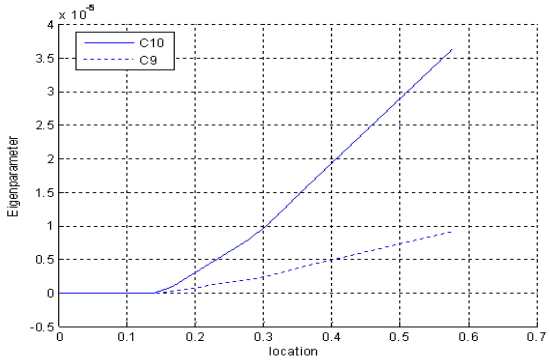

Fig.(15) Eigenparameter for C9,C10 (1st mode)

RESIDUAL ERROR METHOD IN THE MOVEMENT EQUATION:

Error has been presented in the movement equation for damage scenarios and for first three modes as shown in Fig.(16) to Fig.(19), where a positive peak has been displayed at the damaged regions clearly and precisely for all investigated modes and scenarios (single and multiple damage). It is clear that the indication for damage presence will be perceptible when the damage being more sever and closer to the fixed end where the maximum bending has been occurred at this point.

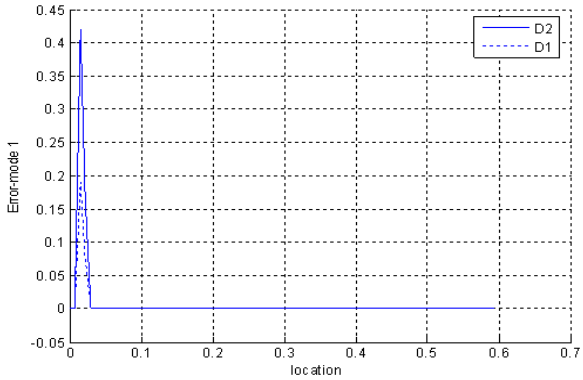

Fig.(16) Residual error for D1,D2 (1st mode)

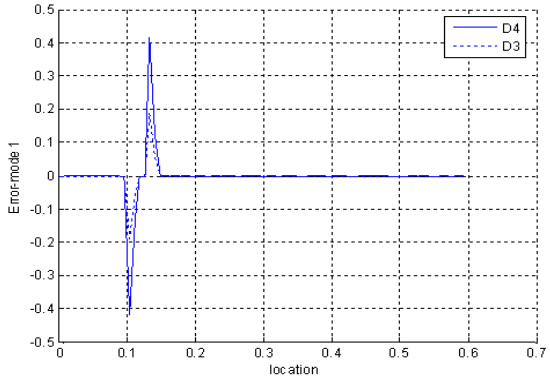

Fig.(17) Residual error for D3,D4 (1st mode)

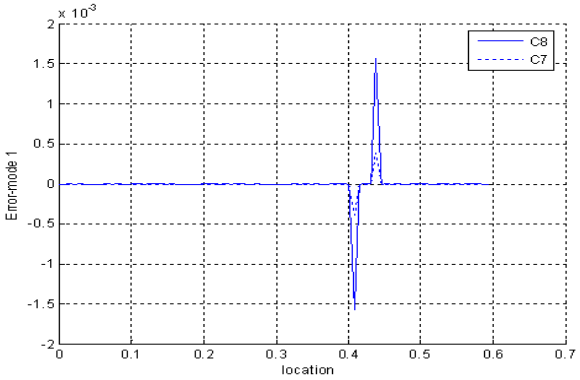

Fig.(18) Residual error for C7,C8 (1st mode)

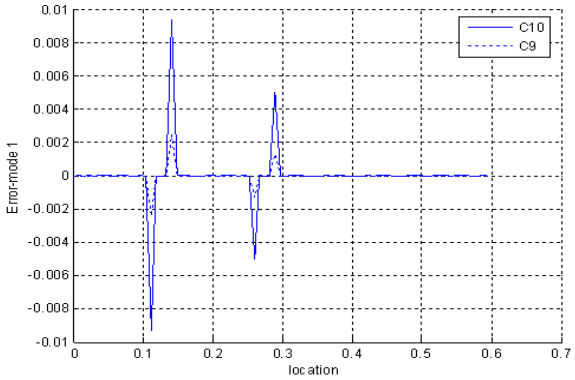

Fig.(19) Residual error for C9,C10 (1st mode)

MODE SHAPE CURVATURE:

The absolute differences between mode shape curvature of healthy and defected blade for the damage scenarios are plotted. For the cases of single damage the maximum difference for each mode shape curvature has been occurred at damaged zone as shown in Fig.(21)and(22) except scenarios (D1,D2,C1 and C2)where the differences of mode shape curvature are localized near the damaged zone (not at the damaged zone) and it is a difficult task to detect the damage which locates close to the fixed end as in Fig(20),For the cases of multiple damage it has been able to locate the damage at two zone,see Fig.(23)

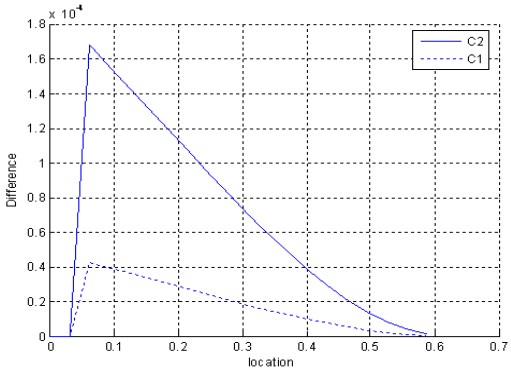

Fig.(20) Absolute diff. for C1,C2 (1st mode)

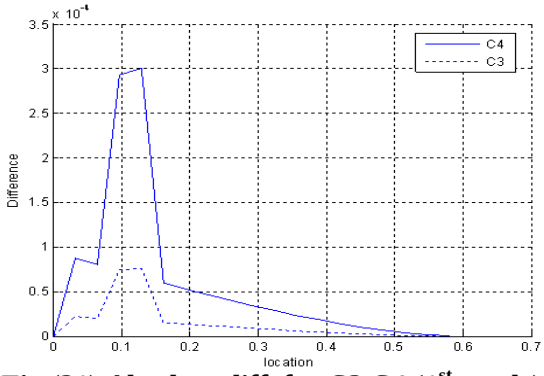

Fig.(21) Absolute diff. for C3,C4 (1st mode)

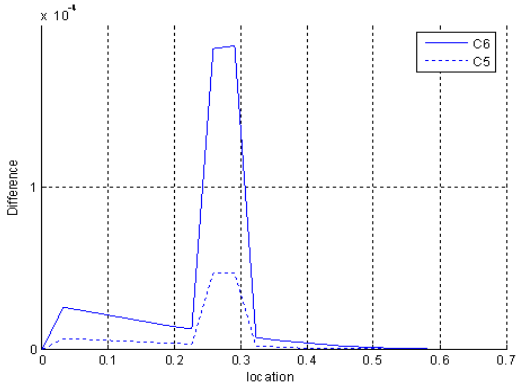

Fig.(22) Absolute diff. for C5,C6 (1st mode)

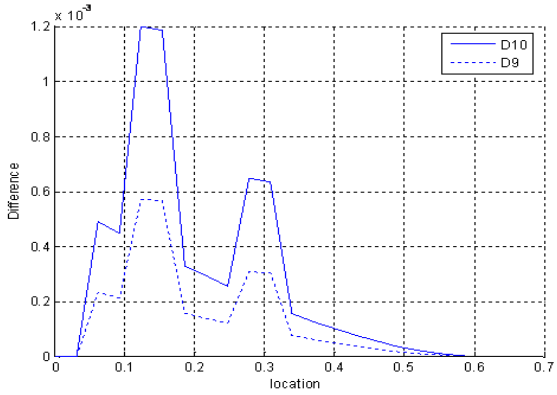

Fig.(23)Absolute diff. for D9,D10 (1st mode)

ROTATION SPEED EFFECT ON DETECTION METHODS:

The effect of rotation speed on detection methods has been investigated for rotation speed scenarios which listed in table (3) for the first mode only because it is the clearest mode to present the facts as shown in Fig. (24-26) .

The effect of rotation speed has been investigated on the first method (as in tables(4) and (5)) and on the other used methods at two values of Ω =(0 and 30) rad/sec, as shown in Fig.(24-26). It is clear that the identification for damage presence under non-rotating conditions noticeable, compared with the identification under rotating conditions, where the centrifugal effect stiffening the blade.

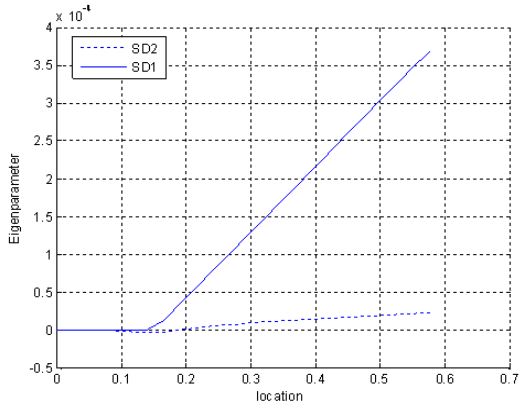

Fig.(24)Eigenparameter for SD1,SD2

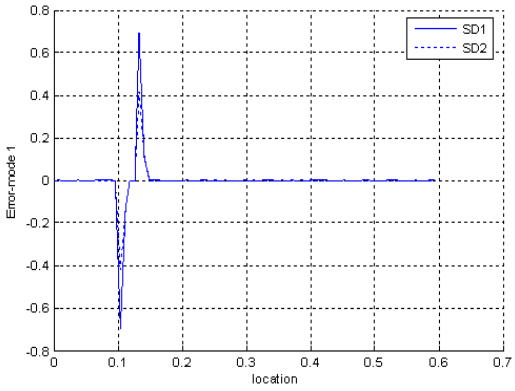

Fig.(25) Residual error for SD1,SD2

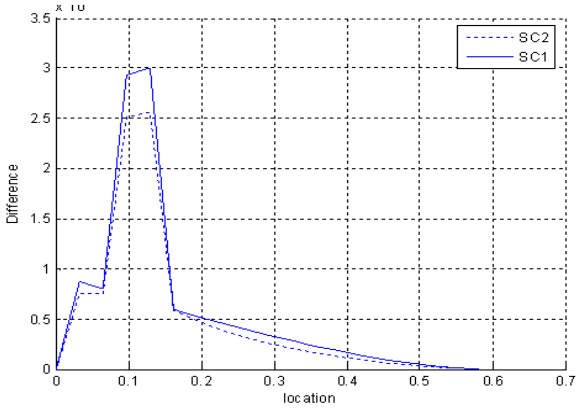

Fig.(26) Mode shape curvature for SC1,SC2

CONCLUSIONS

The main conclusions of the present work according to the results may be summarized as:

- The shifting at natural frequencies only are insufficient to detect the damage , so these frequencies affected by crack depth and stiffness reduction imperceptibly, specially when the damage located far from fixed end, as well as the decreasing in natural frequencies only can not locate the damage .
- The maximum decreasing occurred for the natural frequencies at the severest damage value and the nearest damaged element to the fixed end , and these frequencies decrease with damage accumulation.
- For the same values of damage percent and crack ratio ; the indication for the damage percent case is clearer than the indication for the crack ratio case.
- The natural frequencies increase when the rotational speed increasing , where the centrifugal force stiffening the blade, so the indication for damage presence under non- rotating conditions is clearer than the indication under rotating conditions .
- Residual Error Method in The Movement Equation is very efficient for damage identification, where this method has the ability to identify the damage succefully for the cases of single and multiple damage , so it is effective method to detect and locate the damage.

REFERENCES

- Al-said Samer Masoud, Naji Malak and Al-Shukry Adnan A., (2006). "Flexural vibration of rotating cracked Timoshenko beam". Journal of vibration and control .
- Mohammad H.F. Dado and Omar A. Shpli, (2003). "Crack parameter estimation in structures using finite element modeling". International Journal of solids and structures .
- Ricci P. and Viola E., (2002). "Formulation of the dynamic behavior of cracked plane frame structures". University of Bologna, Viale Risorgimento 2-40136, Bologna, Italy.
- Herrera J. C., (2005). "Evaluation of structural damage identification methods based on dynamic characteristics". A thesis submitted in partial fulfillment of the requirements for the degree of Doctor of Philosophy in civil engineering / University of Puerto Rico.
- Stevens Patricia Lynn, (2001)."Active interrogation of helicopter main rotor faults using trailing edge flap actuation". A thesis submitted in partial fulfillment of the requirements for the degree of Doctor of Philosophy in Mechanical Engineering/The Pennsylvania state university.
- Hodges D. H. and Dowell E. H., (1974). "Nonlinear equations of motion for the elastic bending and torsion of twisted nonuniform rotor blades". Ames Research Center and U. S. Army Air Mobility RED laboratory Moffett Field , Calif. 94035.
- Rao S. S., (1989). "The finite element method in engineering", (Book). Second edition, Purdue university, West Lafayetta, Indiana, USA.
- Thomson W.T, (1975)."Theory of vibration with applications".(Book). University of California, USA, printed in India.
- Meirovitch L., (1975)."Elements of vibration analysis". (Book) International student edition.
- Yuen M. M. F., (1984). "A numerical study of the eigenparameters of a damaged cantilever". Journal of Sound and Vibration 103(3), 301-310.
- Brasiliano A., Doz G. N. and Brito J. L.,(2003). "Damage identification in continuous beams and frame structures using the Residual Error Method in the movement equation". Nuclear Engineering and Design 227, 1-17. Cacciola P., Impollonia N. and Muscolino G., (2003). "Crack detection and location in a damaged beam vibrating under white noise". Comuters and Structures 81, 1773-1782.
- Solaiman Solly, (1999). "Dynamic modeling and stability analysis of a smart Hingeless helicopter blade". A thesis submitted in partial fulfillment of the requirements for the degree of Master of Mechanical Engineering/Carleton university.